ACS Photonics

pubs.acs.org/journal/apchd5

Article

Orbital Angular Momentum Communications in Commercial Multimode Fiber with Strong Mode Coupling

Fengchao Ni,[‖] Zhengyang Mao,[‖] Haigang Liu,* and Xianfeng Chen*

Cite This: *ACS Photonics* 2025, 12, 4423−4431

Read Online

ACCESS | Metrics & More | Article Recommendations | Supporting Information

ABSTRACT: The optical orbital angular momentum (OAM) is regarded as a new dimension for next-generation communication systems for its potential to break the Shannon limit of communication capacity. However, since OAM modes cannot be stably transmitted in conventional fibers, all of the OAM communication schemes proposed so far primarily utilize specialty fibers or multimode fiber (MMF) with weak mode coupling to transmit OAM modes, which hinders the widespread application of OAM communication. Here, we demonstrate the OAM communication in commercial MMF with strong mode coupling by utilizing the transmission matrix (TM) method, for the first time as far as we know. After measuring the TM of MMF, we first experimentally realize the demultiplexing of up to 5 superimposed OAM modes after transmission over MMF with high separation accuracy. Then, the validation of our scheme is further verified by demonstrating dual-channel OAM shift keying and OAM division multiplexing communication in commercial MMF experimentally. This new method exhibits a huge potential for implementing high-capacity and low-crosstalk OAM communication in conventional MMF, which opens a path toward commercial OAM fiber communication and inspires more applications of OAM in commercial MMF.

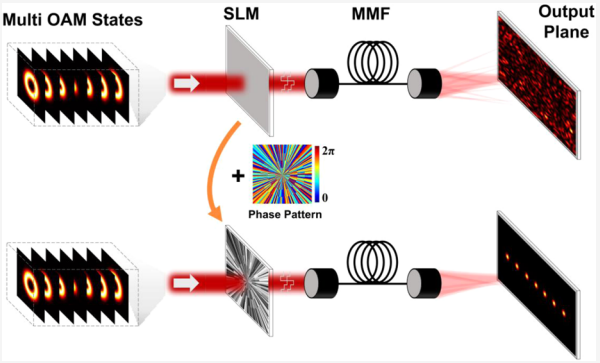

KEYWORDS: *scattering matrix, wavefront shaping, orbital angular momentum, fiber communication, strong coupling*

INTRODUCTION

Over the past 40 years, the optical communication based on polarization,[1−3] wavelength,[4,5] amplitude,[6] and phase[7,8] of light has significantly improved the data-carrying capacity of communication systems. As the capacity of the conventional optical communication system gradually reaches the nonlinear Shannon limit,[9,10] the exploration of new schemes to break the capacity limitation has significant importance.[11,12] The optical orbital angular momentum (OAM), which is carried by optical vortex beams (OV), has been proved to be a promising tool to address the forthcoming capacity crunch.[13−15] OVs have helical phase distributions in their electric fields that are proportional to the azimuthal phase term of $\exp(il\theta)$, where θ is the azimuthal coordinate and l is the topological charge.[16,17] OVs with different l are orthogonal to each other, which makes it possible to use the OAM states as the communication channels.[18,19] More compelling and attractive, in contrast to spin angular momentum (SAM), which has only two states of $\pm\hbar$, the theoretically unlimited values of l provide an infinite number of orthogonal OAM eigenstates, which can infinitely elevate the capacity of a communication system.[20−22] Therefore, there has been enormous enthusiasm on OAM communication.

Depending on the propagation medium of the OAM mode, the OAM communication can be classified into free-space optical (FSO) OAM communication[23−26] and OAM fiber communication.[27−30] Considering that the transmission of light in free space is vulnerable to the environment,[31,32] OAM fiber communication using fibers as mode containers holds greater potential for achieving long-distance OAM communication. Early studies on OAM fiber communication utilized specially designed vortex fibers to achieve stable transmission. The first experimental demonstration of OAM fiber communication was implemented in a specially designed ring core fiber (RCF).[27] Since then, photonic crystal fibers (PCFs),[33,34] air core fibers (ACFs),[35,36] and multicore RCFs[37,38] have been used to realize the OAM fiber communication. All of these works have highlighted the robust capability of OAM modes in expanding communication capacity and have propelled the development of OAM fiber communication.

However, these specially designed vortex fibers exhibit some drawbacks that hinder the commercial use of vortex fibers. The

Received: April 9, 2025
Revised: July 16, 2025
Accepted: July 17, 2025
Published: July 25, 2025

https://doi.org/10.1021/acsphotonics.5c00816
ACS Photonics 2025, 12, 4423−4431

main disadvantage lies in the structure of these special vortex fibers. To support the transmission of OAM modes, vortex fibers usually require complex structures such as a multilayer structure, a multicore structure, or a photonic crystal structure. The complex structures for mode spacing enhancement increase the manufacturing difficulty and reduce the fabrication tolerance. At the same time, the complex fiber structure also necessitates additional materials and more intricate manufacturing processes, which significantly raise the manufacturing costs of the vortex fibers. Besides, many currently widely used optical fiber communication networks are built on traditional multimode fibers (MMFs). The use of specialized vortex fibers leads to compatibility issues and impacts the overall efficiency of fiber systems. Therefore, in order to further promote the practical and commercial application of OAM fiber communication, it is of fundamental importance to realize the OAM communication process in standard commercial MMF. Although some studies have reported OAM communication in MMF with weak mode coupling by utilizing the superposition of MMF's eigenmodes,[39,40] the transmission of OAM modes in MMF is inherently unstable[28] due to the mode coupling effect between different OAM modes. Therefore, in the strong mode coupling regime, such as long-distance transmission, these schemes fail to achieve stable OAM communication due to the increased intermode crosstalk.[41]

In this paper, we demonstrate the OAM communications in commercial MMF with strong mode coupling for the first time to our knowledge. We first measure the OAM-basis transmission matrix (TM) of the MMF, which reveals the physical mechanism of the optical process in MMF and provides an effective method for manipulating the transmission process of OAM modes in MMF. Subsequently, we employ the measured TM to realize the mode conversion between OAM modes in MMF, thereby achieving the demultiplexing of superimposed OAM modes after transmission over the MMF. The corresponding demultiplexing accuracy exceeds 87% under the condition of 5 multiplexed OAM modes. To further illustrate the validity and feasibility of our scheme, we implement both the OAM shift keying (OAM-SK) communication with a low symbol error rate (SER) of about 5% and the OAM division multiplexing (OAM-DM) communication in commercial MMF with low crosstalk. The experimental results verify the success of our scheme in utilizing the TM method to realize the OAM communication in commercial MMF with strong mode coupling. As a result, our demonstration presents a viable approach for the demultiplexing of overlay OAM modes transmitted over MMF, paving the way for practical OAM fiber communication.

THEORY

In a typical MMF excited by monochromatic light, coupling between modes significantly interferes with the transmission process within the fiber. Highly structured patterns can be detected at the output of the fiber, similar to those observed in scattering media. For this reason, wavefront shaping techniques widely used in modulating scattering media can be applied to control the transmission of light[41−43] or even transmit images[44] through fibers, including the TM method. The TM method for MMF indicates that the light field at the output of MMF is related to the input field through a TM, which is written by

$$E_m^{\text{out}} = \sum_{n=1}^{N} k_{mn} E_n^{\text{in}} \tag{1}$$

where k_{mn} is the element of the TM. E_m^{out} is the mth mode of the output field, and E_n^{in} is the nth mode of the input field. The measurement of the TM requires the use of a complete set of orthogonal bases, with the Hadamard base being the most commonly employed. OAM modes also form a complete set of orthogonal bases, and the corresponding measured TM is referred to as the OAM-basis TM, which allows for better modulation of the transmission of OAM modes.[45] Therefore, we construct the OAM-basis TM by using N OAM modes as the orthogonal base, which is written by

$$Y_{FS}^{\text{out}} = K_{\text{OAM}} \cdot X_{\text{OAM}}^{\text{in}} \tag{2}$$

where $Y_{FS}^{\text{out}} = [y_1^{\text{out}}, \cdots, y_N^{\text{out}}]$ is the output matrix, $X_{\text{OAM}}^{in} = [x_1^{\text{in}}, \cdots, x_N^{\text{in}}]$ is the input matrix, and K_{OAM} is the OAM-basis TM. The output matrix and the input matrix refer to the complex amplitude distribution of the light field. In the experiment, we use a spatial light modulator (SLM) to modulate the input field to match the input matrix. The subscripts FS and OAM indicate which Hilbert space the matrix belongs to. $X_{\text{OAM}}^{\text{in}}$ is an identity matrix because x_n^{in} is the eigen vector in OAM space. TM is a complex matrix containing both amplitude and phase terms. However, the existing detectors are intensity detectors without the ability to directly obtain the phase term. We can measure the TM using a full-field interferometry method such as the four-step phase-shifting method (see Supporting Section I for more details).

Figure 1 illustrates the schematic of OAM demultiplexing in MMF via the TM method. The initial beam is a Gaussian beam. As shown in Figure 1a, the intensity distribution on the output plane after transmission over MMF is chaotic and irregular without modulation by the TM method. After measuring the TM, the optical phase conjugation (OPC)

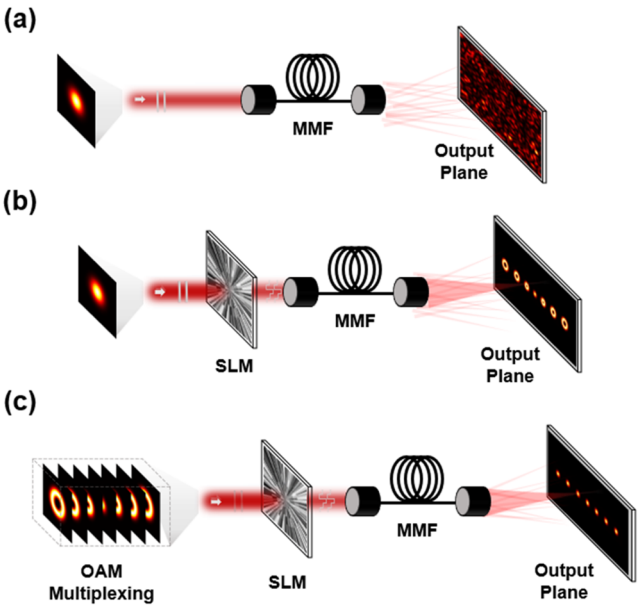

Figure 1. Schematic of OAM demultiplexing in MMF via the TM method. (a) Highly structured speckle patterns without the TM method. (b) Focused OAM array generated by TM. (c) Demultiplexing of superimposed OAM modes.

https://doi.org/10.1021/acsphotonics.5c00816
ACS Photonics 2025, 12, 4423−4431

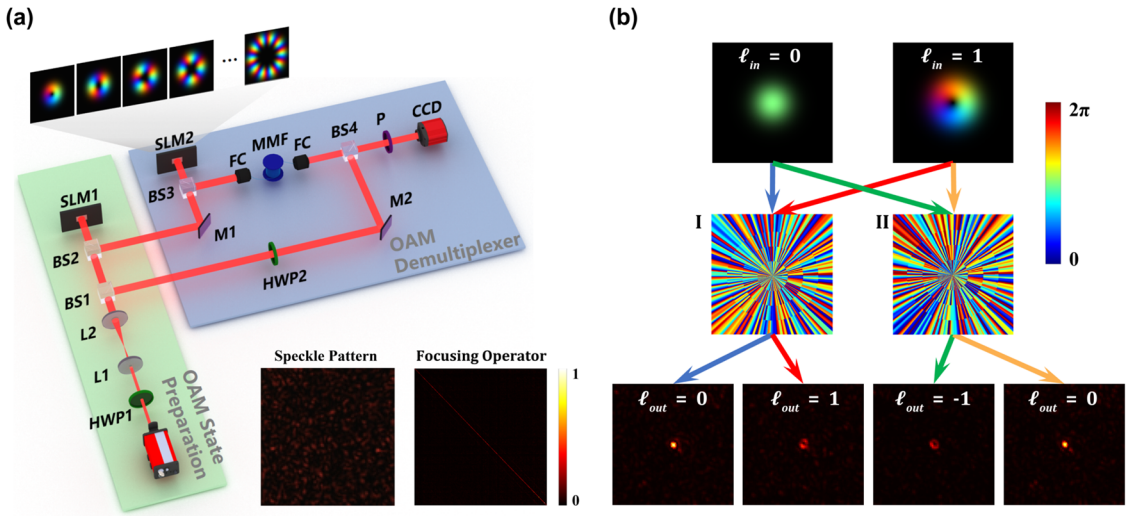

Figure 2. OAM demultiplexing in MMF via the TM method. (a) Experimental setup. P, polarizer; HWP, half wavelength plate; L1−2, lens, f1−2 = 30, 200 mm; BS, beam splitter; SLM, spatial light modulator; M, reflecting mirror; FC, fiber coupler; MMF, multimode fiber. The insets at the bottom show the speckle pattern and the focusing operator of measured OAM-basis TM, respectively. (b) Conversion between different OAM modes in MMF.

method can be adopted to realize the focusing of the Gaussian beam on an arbitrary position. The input matrix is given by

$$X_{\mathrm{OAM}}^{\mathrm{in}} = K_{\mathrm{OAM}}^{\dagger} \cdot Y_{FS}^{\mathrm{target}} \tag{3}$$

where Y_{FS}^{target} corresponds to the target intensity distribution on the output plane that is a Gaussian focus. And the corresponding output field after loading the input matrix $X_{\mathrm{OAM}}^{\mathrm{in}}$ is

$$Y_{\mathrm{OAM}}^{\mathrm{out}} = K_{\mathrm{OAM}} \cdot X_{\mathrm{OAM}}^{\mathrm{in}} = K_{\mathrm{OAM}} \cdot K_{\mathrm{OAM}}^{\dagger} \cdot Y_{FS}^{\mathrm{target}} \approx \chi I \cdot Y_{FS}^{\mathrm{target}} \tag{4}$$

where $K_{\mathrm{OAM}} \cdot K_{\mathrm{OAM}}^{\dagger} \approx \chi I$, indicating that the output field is consistent with the target field. Since X_{OAM}^{in} obtained here is the distribution in OAM space, we need to convert it to a spatial distribution matrix by

$$E_{m,FS}^{\mathrm{in}} = \sum_{n=1}^{N} k_{mn}^{*} x_{n}^{\mathrm{in}} \tag{5}$$

where k_{mn}^{*} represents the conjugation of the elements of K_{OAM}. The TM method tells us that as long as the complex amplitude distribution of the input beam in free space matches the obtained input matrix $E_{m,FS}^{\mathrm{in}}$, a Gaussian focus can be achieved at the output field. If we add extra $l\hbar$ OAM to eq 5, the Gaussian focus will be transformed into a focused OAM spot with a topological charge of l. The corresponding input matrix is

$$E_{m,FS}^{l} = \sum_{n=1}^{N-l} k_{mn}^{*} x_{n+l}^{\mathrm{in}} \tag{6}$$

So far, we have used the TM method to achieve the conversion from the initial Gaussian mode to an arbitrary single OAM mode. Furthermore, we calculate O different input matrices that correspond to O different focused OAM modes and then average them to obtain the final input matrix, which is written by

$$E^{\mathrm{final}} = \sum_{p=1}^{O} E^{l_p} \tag{7}$$

This final input matrix E^{final} can create an OAM array composed of O different OAM modes with arbitrary positions and topological charges l_p, as shown in Figure 1b. If the initial beam is multiplexed vortex beams rather than a Gaussian beam, similar to the traditional antitopological charge matching method,[25,46] the focused OAM spots matching the incident OAM mode will be transformed into Gaussian-like foci, thereby achieving the OAM mode demultiplexing in MMF, as shown in Figure 1c.

RESULTS

OAM Demultiplexing in MMF. With the proposed TM method, the demultiplexing of superimposed OAM modes in MMF can be performed experimentally. The corresponding results are shown in Figure 2, in which Figure 2a shows the experimental setup. Overall, the experimental setup can be divided into the OAM state preparation module and the OAM demultiplexer module. The light source is a linearly polarized continuous laser at the wavelength of λ = 671 *nm*. A half-wave plate (HWP1) after the laser is used to adjust the polarization of the laser beam to the horizontal direction. The laser beam is then expanded by a pair of lenses. The expanded beam is split into a signal beam and a reference beam by BS1. There are two-phase-only spatial light modulators (SLMs, 1920 × 1200 pixels, UPOLabs HDSLM80R) to continuously modulate the signal beam, where SLM1 is used to generate superimposed OAM modes and SLM2 is used to load the input matrix. After being modulated by SLM2, the shaped signal beam is coupled into the commercial MMF with a length of 1 *m*. To introduce strong mode coupling, we choose a fiber with a large core diameter of 100 μm and apply stress to it. After transmission over the MMF, the output beam is combined with the reference beam via BS4. The intensity distribution of the interference field is imaged by a charge-coupled device camera (CCD, DAHENG IMAGING MER-131−210U3M/C). When transmitting OAM mode directly, the camera will capture

https://doi.org/10.1021/acsphotonics.5c00816
ACS Photonics 2025, 12, 4423−4431

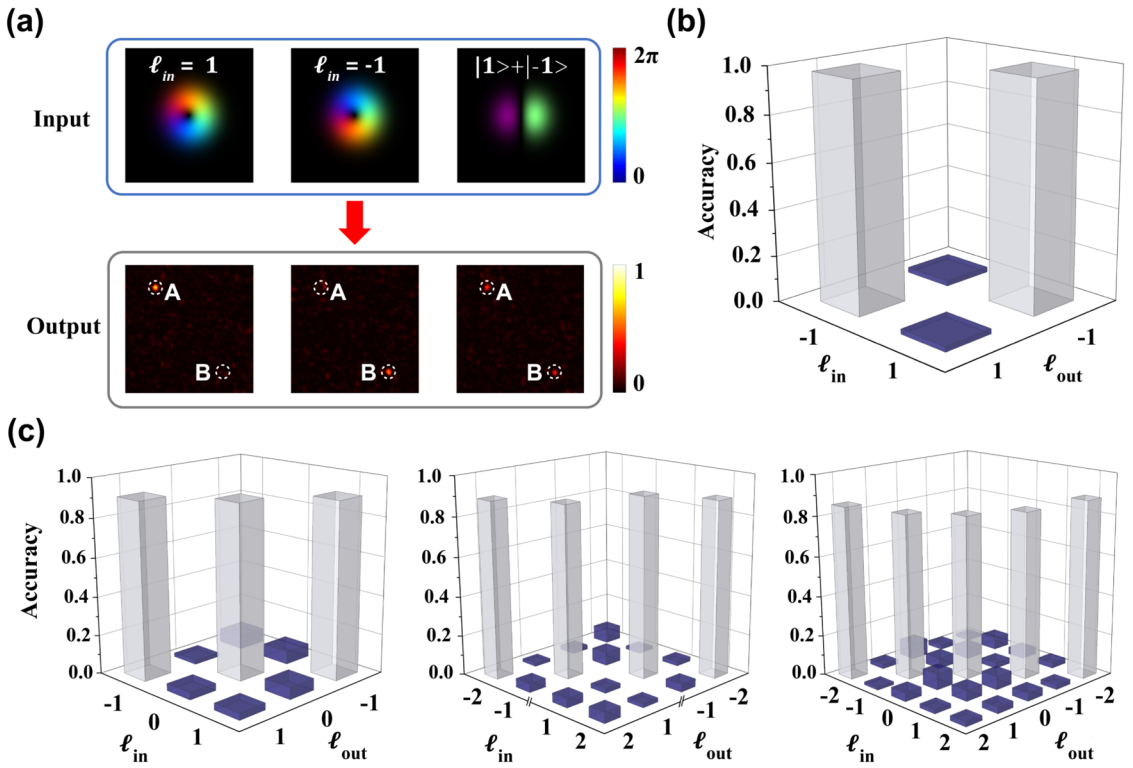

Figure 3. Demultiplexing of superimposed OAM modes after transmission over MMF. (a) Demultiplexing of superimposed OAM modes consisting of 2 OAM modes with $l = \pm 1$. (b) Corresponding separation accuracy. (c) Separation accuracies of 3, 4, and 5 overlay OAM modes.

speckle patterns as shown in the inset at the bottom of Figure 2a, which confirms the presence of strong mode coupling. The reference beam is introduced to implement the four-step phase-shifting method, which is removed after measuring the TM. To measure the OAM-basis TM, we selected $N = 804$ LG modes as the input basis vectors, with the radial index values ranging from 0 to 3 and the angular index values ranging from −100 to +100. Some of the LG modes are shown in the inset at the top of Figure 2a. The modulation capability of the measured TM can be characterized using the focusing operator $K_{\mathrm{OAM}} \cdot K_{\mathrm{OAM}}^{\dagger}$. The inset at the bottom right of Figure 2a shows the $K_{\mathrm{OAM}} \cdot K_{\mathrm{OAM}}^{\dagger}$ of our measured TM, in which the uniform strong diagonal distribution indicates that the measured TM can generate focal points with nearly equal intensity at any position on the output plane.

We first achieve the conversion between different OAM modes in MMF via the TM method, as shown in Figure 2b. As a proof of concept, the input beam is a single OAM mode with $l = 0$ or $l = 1$. The two-phase patterns computed by eq 6 achieve the conversion from the input Gaussian beam to Gaussian focus (labeled by I) and focused OAM spot with $l = -1$ (labeled by II), respectively. The last line shows the intensity distribution of the output beam transmitted over the MMF. There are four different scenarios presented, with each experimental path represented by a distinct color. The results are clearly consistent with our expectations. By loading pattern I to SLM2, the input mode is only focused without mode conversion. If the loading pattern is II, as discussed above, there will be an additional OAM with $l = -1$ added to the input mode. The input OAM mode with $l = 0$ will be converted to a focused OAM spot with $l = -1$, while the input OAM mode with $l = 1$ will become a Gaussian focus. Similar to the antitopological charge-matching method widely used in OAM communication, the result indicates the ability of our method to demultiplex OAM modes in MMF.

We further demonstrate the demultiplexing of 2 superimposed OAM modes with $l = \pm 1$ after transmission over MMF, as shown in Figure 3a. The function of the loaded phase pattern is to simultaneously generate a focused OAM spot with $l = -1$ at position A and a focused OAM spot with $l = 1$ at position B, which is calculated by eq 7. Consequently, when the input mode is single OAM mode with $l = 1$, a Gaussian focus is formed at position A, and at position B, a focused vortex spot with $l = 2$ is also formed. However, due to the lower enhancement factor, no significant vortex-shaped focus is observed. Similarly, when the topological charge of the input OAM mode is − 1, a Gaussian focus will form at position B. And when the input mode is the superposition of these two OAM modes, these two OAM modes are, respectively, converted to Gaussian focus at position A and position B, thereby realizing the demultiplexing of them. Figure 3b shows the corresponding separation accuracy P_n for separating the OAM mode with l_n, which is defined by

$$P_n = \frac{I_n}{\sum_m I_m} \tag{8}$$

where I is the average intensity of the separating region corresponding to the OAM mode with l_n, that is, the white dashed circle at position A for the OAM mode with $l = 1$. And the subscript m denotes that the topological charge of the input mode is l_m. The corresponding separation accuracies for 2 overlap OAM modes are both more than 97%, as shown in Figure 3b. Moreover, we investigate its ability to separate the overlap OAM modes composed of more modes. Figure 3c illustrates the demultiplexing results of 3, 4, and 5 overlap OAM modes, with the corresponding separation accuracy

https://doi.org/10.1021/acsphotonics.5c00816
ACS Photonics 2025, 12, 4423−4431

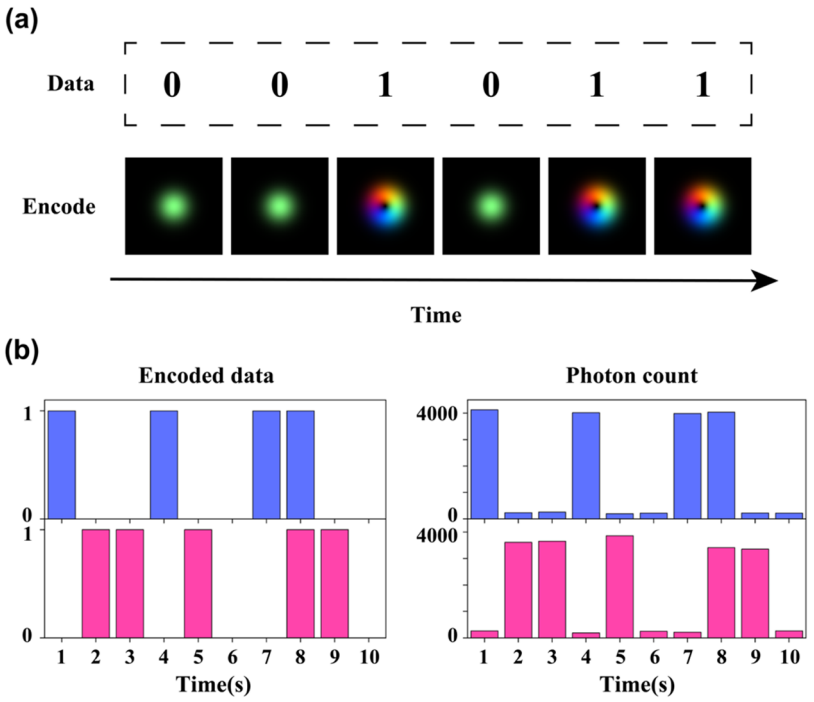

Figure 4. Dual-channel OAM-SK communication in MMF. (a) Coding rule of OAM-SK. (b) Encoded data to be transmitted and the variation of photon counts in the two channels. The data can be decoded by the photon count.

reaching over 95, 90, and 87%, respectively. As the number of overlap modes increases, the separation accuracy gradually decreases, which is primarily due to the same amount of energy being distributed across multiple spatial regions, resulting in decreased energy per point. We also demonstrate the demultiplexing of 2 overlap OAM modes with different phases, which shows the tolerance of our method to phase (see Supporting Section II). The above results are repeatable, which confirms the validity and stability of our TM method to realize the OAM demultiplexing in MMF.

OAM-SK and OAM-DM Communication in MMF. The result of OAM demultiplexing via the TM method demonstrates its potential to realize OAM communication in MMF. To more comprehensively demonstrate the application potential of our method, in this section, we present the experimental results of both OAM-SK communication and OAM-DM communication in MMF via the TM method. For OAM-SK communication, the OAM mode is regarded as a modulation format that enables the encoding of information by dynamic switching of OAM modes.[47,48] For OAM-DM communication, vortex beams carrying OAM are regarded as carriers of signal, where different vortex modes correspond to different communication channels.[25,27]

Figure 4 illustrates the result of OAM-SK communication in MMF. The detailed binary coding rule is shown in Figure 4a. A 6-bit binary byte "001011" is encoded by using OAM mode with $l = 1$. Each bit value is assigned to be 1 or 0 on the basis of whether the OAM mode exists or not. OAM mode is continuously varying in the time domain to form the whole byte. As proof of principle, we present a dual-channel OAM-SK communication experiment here. We transmit a 10-bit binary byte "1001001100" in Channel 1 encoded by OAM mode with $l = 1$ and "0110100110" in Channel 2 encoded by OAM mode with $l = -1$. For the simultaneous modulation of these two channels, the signal beam is divided into two beams, with each beam incident on the left or right region of SLM1 for different OAM encoding. The phase patterns in SLM1 change over time. After loading the demultiplexing phase pattern on SLM2, the obtained Gaussian focus at the output of MMF is filtered out by the pinhole and collected by a single-photon detector (SPD) (see Supporting Section III for details about the setup). The decoding of information can be achieved by analyzing the photon count detected by SPD. For Channel 1, if the loaded bit is "1" (input OAM mode with $l = 1$), the generated Gaussian focus will lead to a sharply increased photon count. By contrast, if the loaded bit is "0," the photon count is very low due to the vortex-shaped focus with low intensity in the center, and the same applies to Channel 2. The experimental result is shown in Figure 4b, in which the blue columns represent Channel 1 and the red columns represent Channel 2. For both channels, the SPD can collect around 4000 photons per second under the condition of bit "1," while for bit "0," the photon count drops to only about 250 per second. There is an enhancement of over 15 times. By setting a threshold of 2000 photons, we can decode the collected data and achieve very low error rates of about 5% in dual-channel OAM-SK communication. As a proof-of-principle demonstration, our demonstrated OAM-SK experiment exhibits a limited data rate of approximately 1 bit per second (bps), which is a common limitation of the OAM-SK communication scheme. Further enhancement of the data rate is possible by utilizing modulators with higher modulation speeds, such as a digital micromirror device (DMD) spatial light modulator, which is capable of operating at speeds above 10 kHz.

The OAM-DM communication in MMF is also realized via our TM method. We set two multiplexed channels as the proof-of-principle experiment. The OAM state preparation module is adjusted to consist of two identical lasers at the wavelength of $\lambda = 520\ nm$. One path of the laser beam is modulated using the internal amplitude modulation of the laser

https://doi.org/10.1021/acsphotonics.5c00816
ACS Photonics 2025, 12, 4423−4431

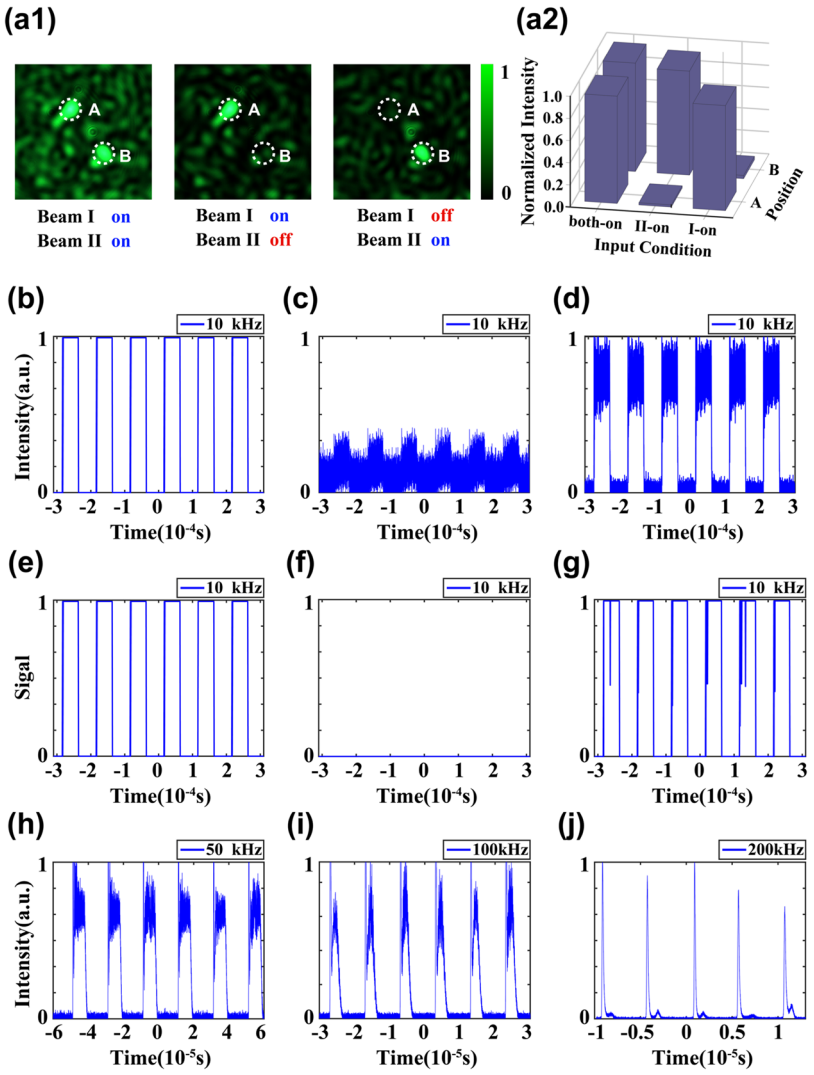

Figure 5. Dual-channel OAM-DM communication in MMF. (a1) Demultiplexing results with different beams on. (a2) Numerical results of the normalized intensity at positions A and B under different input conditions. (b) Loaded square wave signal at 10 kHz. (c, d) Sampled carrier signal at 10 kHz before and after loading the demultiplexing phase pattern. (e−g) Encoded signal and decoded signals before and after loading the demultiplexing phase pattern. (h−j) Sampled carrier signals at different internal modulation frequencies.

to load the square wave signal, which is labeled by beam I. The other path labeled by beam II is not modulated with any signal. These two beams are transformed into different OAM modes with $l = \pm 1$ by different SLMs, which are then multiplexed together to generate the overlap OAM modes. After loading the demultiplexing phase pattern calculated by the TM method, these two beams are converted into different Gaussian foci at the output of MMF. The Gaussian focus corresponding to the modulated signal beam is filtered by a pinhole. Finally, the carrier signal of the filtered beam is sampled by an oscilloscope (see Supporting Section IV for more details).

The corresponding experimental result is illustrated in Figure 5. Figure 5a1 shows the result of demultiplexing. The Gaussian focus corresponding to the modulated OAM beam labeled by beam I is at the position A, and the Gaussian focus corresponding to beam II without modulation is at the position B. In order to more clearly demonstrate the low channel crosstalk, the numerical results of the normalized intensity at positions A and B under different input conditions are illustrated in Figure 5a2. It can be seen that the intensity at position A shows little variation between the I-on and both-on cases, and the corresponding separation accuracy defined by eq 8 is exceeding 95%, indicating a low channel crosstalk. The Gaussian focus at position A is filtered out and sampled by an oscilloscope. The loaded modulation square wave signal at 10 kHz is shown in Figure 5b. The sampled carrier signal of the filtered beam without loading the demultiplexing phase pattern calculated by the TM method is shown in Figure 5c. The chaotic and irregular waveform indicates that the communication process is significantly destroyed by mode-coupling effects in MMF. By contrast, after loading the demultiplexing phase pattern, the sampled carrier signal illustrated in Figure 5d clearly demonstrates the characteristics of a square wave signal. The interval between adjacent signals is 0.1 *ms*, which is consistent with the frequency of the loaded modulation signal. By setting an intensity threshold of 0.5, we can encode the beam with "0" and "1" by the intensity. Figure 5e shows the encoded signal, and Figure 5f,g shows the decoded signal before and after loading the demultiplexing phase pattern. It is clearly seen that after using the TM method, we successfully demultiplex the modulated signal beam from the superimposed OAM modes after transmission over MMF and obtain the

https://doi.org/10.1021/acsphotonics.5c00816
ACS Photonics 2025, 12, 4423−4431

correct decoded signal consistent with the encoded signal. The results verify the success of OAM-DM communication in MMF via the TM method.

For a better demonstration of the performance of OAM-DM communication in MMF via the TM method, we conduct OAM-DM communication experiments at different internal modulation frequencies of the laser. The results of the sampled carrier signals after loading the demultiplexing phase pattern are shown in Figure 5h−j, in which the modulation frequencies are 50, 100, and 200 kHz, respectively. At low modulation frequency, the obtained carrier signal aligns well with the loaded modulation square wave signal. However, as the frequency increases, the quality of the sampled carrier signal gradually deteriorates. Although the periodic information on the signal, namely, the signal interval, remains consistent with the modulation frequency, the shape of the signal no longer maintains a well-defined square form, indicating a significant decrease in the duty cycle. This is mainly due to the inherent limitation of laser's internal modulation that the increased modulation frequency leads to instability in amplitude modulation. This limitation can be improved by using better signal modulators.

DISCUSSION AND CONCLUSIONS

This work demonstrates the demultiplexing of superimposed OAM modes transmitted over MMF and realizes the OAM-SK and OAM-DM communication in MMF with strong mode coupling. There are still some details about our work that need to be discussed. One crucial issue is the communication capacity. In its present form, we only perform the OAM communication process in MMF with only two individual signal channels as proof of principle. However, the number of signal channels can be easily expanded in practical applications as it is determined by the result of OAM demultiplexing. In our experiment, the number of overlay OAM modes that can be effectively demultiplexed is up to 5, which means that, in principle, we can realize the OAM communication in MMF with at least 5 individual signal channels. Considering that different OAM modes are mutually orthogonal and the scattering is a linear process, our TM method theoretically enables the demultiplexing of an infinite number of overlapping OAM modes. However, the practical maximum number of overlapping OAM modes is limited by the finite dimensionality and resolution of the TM. This limitation can be further improved by increasing the number of OAM eigen vectors used to calculate the OAM-basis TM. TM with higher dimensions can better characterize the transmission capability of MMF, thereby enhancing the sorting and demultiplexing ability of TM. Another important issue is the stability of our TM method. The measured TM depends only on the transmission characteristics of the system. When the transmission characteristics of the scattering system change, it may become necessary to measure a new TM applicable to the new scattering system. In our experiment, the 1 m MMF is fixed onto the optical platform, thereby reducing the probability of deformation and ensuring the strong stability of our method. Under other time-varying channel conditions, however, the TM must be updated promptly. Given that our measurement of the TM takes about 3 min, which meets the requirement for basic communication but still falls short of achieving high-speed communication, the temporal stability of our approach cannot be fully guaranteed. Such limitation mainly stems from the refresh rates of SLM and the detector. Therefore, the temporal stability of our method can be improved by using high-speed SLMs and detectors.

Compared to the demultiplexing experiment, the separation effect in the communication experiments is reduced. This is primarily due to the adjustment of the OAM preparation module, in which the generation of overlay OAM modes is achieved by utilizing BS to superimpose two signal beams instead of directly loading the overlap phase patterns. This interference between two signal beams is inevitable and affects the accuracy of the TM. This issue can be resolved by using a pulsed laser and temporally separating the two beams. In theory, the enhancement factor, which is the ratio of intensity at the separation region and the mean intensity of the background, should be comparable to the number of input modes $N = 804$. However, the enhancement factor obtained in demultiplexing is about 105. This is mainly because the spot sizes of OAM modes with different topological charges loaded are inconsistent, which introduces measurement errors and leads to a decrease in the enhancement factor. It is worth noting that in this work, we have focused solely on the control of OAM modes in MMF using the TM method. In fact, a complete TM reveals the response of the scattering medium to various optical properties of the incident light, including the amplitude, phase, and polarization.[49] For other types of structured light, such as vector vortex beams, their characteristics are similarly manifested in dimensions such as polarization and phase, which means they can also be modulated by the TM.[50,51] Therefore, the simultaneous distinction of multiple different dimensions of the optical field in MMF is achievable via the TM method.

In conclusion, we have reported a novel scheme based on TM to realize the OAM communications in commercial MMF with strong mode coupling, for the first time to our best knowledge. In the experiment, we first construct the OAM-basis TM to control the transmission process in MMF. After measuring the TM and calculating the input matrix, we can transfer the input superimposed OAM modes to different Gaussian foci at different positions at the output of MMF, thereby achieving the demultiplexing of overlay OAM modes, similar to the antitopological charge matching. In our experiment, we achieved demultiplexing of up to 5 OAM modes with a separation accuracy exceeding 87%. The validity of our scheme is further illustrated by performing the dual-channel OAM-SK communication and OAM-DM communication experiments. With the ability to realize effective OAM communications in commercial MMF, our work successfully extended the OAM mode container to conventional MMF, holding the promise of enabling high-capacity and long-distance OAM fiber communication. Compared to previous works using vortex fibers with complex structures or only applicable to weak mode coupling regime, our method is more compatible with existing optical fiber communication networks, which paves the way for the practical and commercial application of OAM fiber communication, and contributes to the realization of next-generation OAM fiber communication that break the existing limitation of communication capacity. The utilization of TM also helps us to further understand the physical mechanism of MMF, provides a new solution for controlling the information process in MMF, and may inspire more applications of OAM modes in MMF.

https://doi.org/10.1021/acsphotonics.5c00816
ACS Photonics 2025, 12, 4423−4431

METHODS

Experimental Setup of OAM-SK Communication. The experimental setup is shown in the Supporting Information. The light source is a linearly polarized continuous laser at the wavelength of λ=780 nm. The signal beam obtained after BS1 is divided into two beams by BS2. The two beams are propagated onto the left and right regions of the SLM to obtain different OAM modes, respectively. At the output of MMF, the output beam is further divided into two beams by BS4. One beam is filtered out by a pinhole to extract the intensity of light field on position A and the other beam is filtered out to exact the intensity on position B. We use the photon counts detected by SPD to evaluate the intensity.

Experimental Setup of OAM-DM Communication. The experimental setup is shown in the Supporting Information. The two lasers are both continuous lasers with a wavelength of λ = 532 nm. These two beams are modulated by different SLMs to be transformed into different OAM modes with $l = \pm 1$. The internal modulation of laser 1 modulates the input beam I with a square wave signal. The topological charge of beam I is $l = +1$, while the topological charge of beam II is $l = -1$. BS3 is used to multiplex them to prepare the overlap OAM modes. The following optical path is just the same as those used in previous experiments. There is still an interference path to measure the OAM-basis TM. After loading the demultiplexing phase pattern calculated by the TM method, two different Gaussian focuses are generated at the output plane after transmission over MMF. The Gaussian focus corresponding to the modulated signal beam is filtered by a pinhole. Finally, the carrier signal of the filtered beam is sampled by an oscilloscope.

ASSOCIATED CONTENT

Data Availability Statement

The data that support the findings of this study are available from the corresponding author upon reasonable request.

Supporting Information

The Supporting Information is available free of charge at https://pubs.acs.org/doi/10.1021/acsphotonics.5c00816.

Details about the four-step phase-shifting method; experimental results of the demultiplexing of overlap OAM modes with different phases; experimental setup of OAM-SK communication; experimental setup of OAM-DM communication (PDF)

AUTHOR INFORMATION

Corresponding Authors

Haigang Liu − *State Key Laboratory of Photonics and Communications, School of Physics and Astronomy, Shanghai Jiao Tong University, Shanghai 200240, China; Hefei National Laboratory, Hefei 230088, China*; Email: liuhaigang@sjtu.edu.cn

Xianfeng Chen − *State Key Laboratory of Photonics and Communications, School of Physics and Astronomy, Shanghai Jiao Tong University, Shanghai 200240, China; Hefei National Laboratory, Hefei 230088, China; Shanghai Research Center for Quantum Sciences, Shanghai 201315, China*; orcid.org/0000-0002-1301-7448; Email: xfchen@sjtu.edu.cn

Authors

Fengchao Ni − *State Key Laboratory of Photonics and Communications, School of Physics and Astronomy, Shanghai Jiao Tong University, Shanghai 200240, China*

Zhengyang Mao − *State Key Laboratory of Photonics and Communications, School of Physics and Astronomy, Shanghai Jiao Tong University, Shanghai 200240, China*

Complete contact information is available at: https://pubs.acs.org/10.1021/acsphotonics.5c00816

Author Contributions

‖F.N. and Z.M. contributed equally to this work.

Notes

The authors declare no competing financial interest.

ACKNOWLEDGMENTS

F.N. and Z.M. contributed equally to this work. The authors would like to acknowledge support from the National Natural Science Foundation of China (Nos. 121922502 and 12374314), the National Key Research and Development Program of China (No. 2023YFA1407200), and the Innovation Program for Quantum Science and Technology (No. 2021ZD0300802).

REFERENCES

(1) Gnauck, A. H.; Winzer, P. J.; Chandrasekhar, S.; Liu, X.; Zhu, B.; Peckham, D. W. Spectrally Efficient Long-Haul WDM Transmission Using 224-Gb/s Polarization-Multiplexed 16-QAM. *J. Lightwave Technol.* **2011**, *29* (4), 373−377.

(2) Richter, T.; Palushani, E.; Schmidt-Langhorst, C.; Ludwig, R.; Molle, L.; Nolle, M.; Schubert, C. Transmission of Single-Channel 16-QAM Data Signals at Terabaud Symbol Rates. *J. Lightwave Technol.* **2012**, *30* (4), 504−511.

(3) Zhou, X.; Yu, J.; Huang, M.-F.; Shao, Y.; Wang, T.; Nelson, L.; Magill, P.; Birk, M.; Borel, P. I.; Peckham, D. W.; et al. 64-Tb/s, 8 b/s/Hz, PDM-36QAM Transmission Over 320 km Using Both Pre- and Post-Transmission Digital Signal Processing. *J. Lightwave Technol.* **2011**, *29* (4), 571−577.

(4) Kuramochi, E.; Nozaki, K.; Shinya, A.; Takeda, K.; Sato, T.; Matsuo, S.; Taniyama, H.; Sumikura, H.; Notomi, M. Large-scale integration of wavelength-addressable all-optical memories on a photonic crystal chip. *Nat. Photonics* **2014**, *8* (6), 474−481.

(5) Luo, L.-W.; Ophir, N.; Chen, C. P.; Gabrielli, L. H.; Poitras, C. B.; Bergmen, K.; Lipson, M. WDM-compatible mode-division multiplexing on a silicon chip. *Nat. Commnun.* **2014**, *5* (1), No. 3069.

(6) Oubei, H. M.; Duran, J. R.; Janjua, B.; Wang, H.-Y.; Tsai, C.-T.; Chi, Y.-C.; Ng, T. K.; Kuo, H.-C.; He, J.-H.; Alouini, M.-S.; et al. 4.8 Gbit/s 16-QAM-OFDM transmission based on compact 450-nm laser for underwater wireless optical communication. *Opt. Express* **2015**, *23* (18), 23302−23309.

(7) Grimm, A.; Frattini, N. E.; Puri, S.; Mundhada, S. O.; Touzard, S.; Mirrahimi, M.; Girvin, S. M.; Shankar, S.; Devoret, M. H. Stabilization and operation of a Kerr-cat qubit. *Nature* **2020**, *584* (7820), 205−209.

(8) Tang, Z.; Liao, Z.; Xu, F.; Qi, B.; Qian, L.; Lo, H.-K. Experimental Demonstration of Polarization Encoding Measurement-Device-Independent Quantum Key Distribution. *Phys. Rev. Lett.* **2014**, *112* (19), No. 190503.

(9) Kikuchi, K. Fundamentals of Coherent Optical Fiber Communications. *J. Lightwave Technol.* **2016**, *34* (1), 157−179.

(10) Shannon, C. E. A mathematical theory of communication. *Bell Syst. Technol. J.* **1948**, *27* (3), 379−423.

(11) Essiambre, R. J.; Tkach, R. W. Capacity Trends and Limits of Optical Communication Networks. *Proc. IEEE* **2012**, *100* (5), 1035−1055.

(12) Winzer, P. J. Making spatial multiplexing a reality. *Nat. Photonics* **2014**, *8* (5), 345−348.
(13) Lei, T.; Zhang, M.; Li, Y.; Jia, P.; Liu, G. N.; Xu, X.; Li, Z.; Min, C.; Lin, J.; Yu, C.; et al. Massive individual orbital angular momentum channels for multiplexing enabled by Dammann gratings. *Light Sci. Appl.* **2015**, *4* (3), No. e257.
(14) Vallone, G.; D'Ambrosio, V.; Sponselli, A.; Slussarenko, S.; Marrucci, L.; Sciarrino, F.; Villoresi, P. Free-Space Quantum Key Distribution by Rotation-Invariant Twisted Photons. *Phys. Rev. Lett.* **2014**, *113* (6), No. 060503.
(15) Willner, A. E.; Huang, H.; Yan, Y.; Ren, Y.; Ahmed, N.; Xie, G.; Bao, C.; Li, L.; Cao, Y.; Zhao, Z.; et al. Optical communications using orbital angular momentum beams. *Adv. Opt. Photon.* **2015**, *7* (1), 66−106.
(16) Shen, Y.; Wang, X.; Xie, Z.; Min, C.; Fu, X.; Liu, Q.; Gong, M.; Yuan, X. Optical vortices 30 years on: OAM manipulation from topological charge to multiple singularities. *Light Sci. Appl.* **2019**, *8* (1), No. 90.
(17) Allen, L.; Beijersbergen, M. W.; Spreeuw, R. J. C.; Woerdman, J. P. Orbital angular momentum of light and the transformation of Laguerre-Gaussian laser modes. *Phys. Rev. A* **1992**, *45* (11), 8185−8189.
(18) Gröblacher, S.; Jennewein, T.; Vaziri, A.; Weihs, G.; Zeilinger, A. Experimental quantum cryptography with qutrits. *New J. Phys.* **2006**, *8* (5), No. 75.
(19) Mair, A.; Vaziri, A.; Weihs, G.; Zeilinger, A. Entanglement of the orbital angular momentum states of photons. *Nature* **2001**, *412* (6844), 313−316.
(20) Gibson, G.; Courtial, J.; Padgett, M. J.; Vasnetsov, M.; Pas'ko, V.; Barnett, S. M.; Franke-Arnold, S. Free-space information transfer using light beams carrying orbital angular momentum. *Opt. Express* **2004**, *12* (22), 5448−5456.
(21) Shapiro, J. H.; Guha, S.; Erkmen, B. Ultimate channel capacity of free-space optical communications [Invited]. *J. Opt. Networking* **2005**, *4* (8), 501−516.
(22) Franke-Arnold, S.; Allen, L.; Padgett, M. Advances in optical angular momentum. *Laser Photonics Rev.* **2008**, *2* (4), 299−313.
(23) Djordjevic, I. B.; Arabaci, M. LDPC-coded orbital angular momentum (OAM) modulation for free-space optical communication. *Opt. Express* **2010**, *18* (24), 24722−24728.
(24) Tan, H.; Deng, J.; Zhao, R.; Wu, X.; Li, G.; Huang, L.; Liu, J.; Cai, X. A Free-Space Orbital Angular Momentum Multiplexing Communication System Based on a Metasurface. *Laser Photonics Rev.* **2019**, *13* (6), No. 1800278.
(25) Wang, J.; Yang, J.-Y.; Fazal, I. M.; Ahmed, N.; Yan, Y.; Huang, H.; Ren, Y.; Yue, Y.; Dolinar, S.; Tur, M.; Willner, A. E. Terabit free-space data transmission employing orbital angular momentum multiplexing. *Nat. Photonics* **2012**, *6* (7), 488−496.
(26) Wang, J.; Liu, J.; Li, S.; Zhao, Y.; Du, J.; Zhu, L. Orbital angular momentum and beyond in free-space optical communications. *Nanophotonics* **2022**, *11* (4), 645−680.
(27) Bozinovic, N.; Yue, Y.; Ren, Y.; Tur, M.; Kristensen, P.; Huang, H.; Willner, A. E.; Ramachandran, S. Terabit-Scale Orbital Angular Momentum Mode Division Multiplexing in Fibers. *Science* **2013**, *340* (6140), 1545−1548.
(28) Wang, J.; Zhang, X. Orbital Angular Momentum in Fibers. *J. Lightwave Technol.* **2023**, *41* (7), 1934−1962.
(29) Wen, Y.; Chremmos, I.; Chen, Y.; Zhu, G.; Zhang, J.; Zhu, J.; Zhang, Y.; Liu, J.; Yu, S. Compact and high-performance vortex mode sorter for multi-dimensional multiplexed fiber communication systems. *Optica* **2020**, *7* (3), 254−262.
(30) Zhang, J.; Liu, J.; Shen, L.; Zhang, L.; Luo, J.; Liu, J.; Yu, S. Mode-division multiplexed transmission of wavelength-division multiplexing signals over a 100-km single-span orbital angular momentum fiber. *Photonics Res.* **2020**, *8* (7), 1236−1242.
(31) Paterson, C. Atmospheric Turbulence and Orbital Angular Momentum of Single Photons for Optical Communication. *Phys. Rev. Lett.* **2005**, *94* (15), No. 153901.
(32) Krenn, M.; Fickler, R.; Fink, M.; Handsteiner, J.; Malik, M.; Scheidl, T.; Ursin, R.; Zeilinger, A. Communication with spatially modulated light through turbulent air across Vienna. *New J. Phys.* **2014**, *16* (11), No. 113028.
(33) Wong, G. K. L.; Kang, M. S.; Lee, H. W.; Biancalana, F.; Conti, C.; Weiss, T.; Russell, P. S. J. Excitation of Orbital Angular Momentum Resonances in Helically Twisted Photonic Crystal Fiber. *Science* **2012**, *337* (6093), 446−449.
(34) Xi, X. M.; Wong, G. K. L.; Frosz, M. H.; Babic, F.; Ahmed, G.; Jiang, X.; Euser, T. G.; Russell, P. S. J. Orbital-angular-momentum-preserving helical Bloch modes in twisted photonic crystal fiber. *Optica* **2014**, *1* (3), 165−169.
(35) Brunet, C.; Vaity, P.; Messaddeq, Y.; LaRochelle, S.; Rusch, L. A. Design, fabrication and validation of an OAM fiber supporting 36 states. *Opt. Express* **2014**, *22* (21), 26117−26127.
(36) Gregg, P.; Kristensen, P.; Ramachandran, S. Conservation of orbital angular momentum in air-core optical fibers. *Optica* **2015**, *2* (3), 267−270.
(37) Liu, J.; Zhang, J.; Liu, J.; Lin, Z.; Li, Z.; Lin, Z.; Zhang, J.; Huang, C.; Mo, S.; Shen, L.; et al. 1-Pbps orbital angular momentum fibre-optic transmission. *Light Sci. Appl.* **2022**, *11* (1), No. 202.
(38) Zhang, J.; Lin, Z.; Liu, J.; Liu, J.; Lin, Z.; Mo, S.; Lin, S.; Shen, L.; Zhang, L.; Chen, Y.; et al. SDM transmission of orbital angular momentum mode channels over a multi-ring-core fibre. *Nanophotonics* **2022**, *11* (4), 873−884.
(39) Guan, Z.; Zuo, T.; Xie, C.; Huang, L.; Wen, K.; Wang, C.; Ye, H.; Dong, Z.; Fan, D.; Chen, S. Orbital angular momentum mode multiplexing communication in multimode fibers. *Opt. Commun.* **2024**, *569*, No. 130857.
(40) Wang, J.; Chen, S.; Liu, J. Orbital angular momentum communications based on standard multi-mode fiber (invited paper). *APL Photonics* **2021**, *6* (6), No. 060804.
(41) Xiong, W.; Ambichl, P.; Bromberg, Y.; Redding, B.; Rotter, S.; Cao, H. Spatiotemporal Control of Light Transmission through a Multimode Fiber with Strong Mode Coupling. *Phys. Rev. Lett.* **2016**, *117* (5), No. 053901.
(42) N'Gom, M.; Norris, T. B.; Michielssen, E.; Nadakuditi, R. R. Mode control in a multimode fiber through acquiring its transmission matrix from a reference-less optical system. *Opt. Lett.* **2018**, *43* (3), 419−422.
(43) Defienne, H.; Barbieri, M.; Walmsley, I. A.; Smith, B. J.; Gigan, S. Two-photon quantum walk in a multimode fiber. *Sci. Adv.* **2016**, *2* (1), No. e1501054.
(44) Choi, Y.; Yoon, C.; Kim, M.; Yang, T. D.; Fang-Yen, C.; Dasari, R. R.; Lee, K. J.; Choi, W. Scanner-Free and Wide-Field Endoscopic Imaging by Using a Single Multimode Optical Fiber. *Phys. Rev. Lett.* **2012**, *109* (20), No. 203901.
(45) Zhang, H.; Zhang, B.; Liu, Q. OAM-basis transmission matrix in optics: a novel approach to manipulate light propagation through scattering media. *Opt. Express* **2020**, *28* (10), 15006−15015.
(46) Chen, Q.; Qu, G.; Yin, J.; Wang, Y.; Ji, Z.; Yang, W.; Wang, Y.; Yin, Z.; Song, Q.; Kivshar, Y.; Xiao, S. Highly efficient vortex generation at the nanoscale. *Nat. Nanotechnol.* **2024**, *19*, 1000−1006.
(47) Liu, Z.; Yan, S.; Liu, H.; Chen, X. Superhigh-Resolution Recognition of Optical Vortex Modes Assisted by a Deep-Learning Method. *Phys. Rev. Lett.* **2019**, *123* (18), No. 183902.
(48) Dahai, Y.; Jie, L.; Chen, C.; Chang, L.; Junbo, H.; Baiying, L.; Keya, Z.; Yiqun, W.; Peng, J. Multiwavelength high-order optical vortex detection and demultiplexing coding using a metasurface. *Adv. Photonics Nexus* **2022**, *1* (1), No. 016005.
(49) van Rossum, M. C. W.; Nieuwenhuizen, T. M. Multiple scattering of classical waves: microscopy, mesoscopy, and diffusion. *Rev. Mod. Phys.* **1999**, *71* (1), 313−371.
(50) Shao, R.; Ding, C.; Qu, Y.; Liu, L.; He, Q.; Wu, Y.; Yang, J. Full-polarization angular spectrum modeling of scattered light modulation. *Photonics Res.* **2024**, *12* (3), 485−490.
(51) Ding, C.; Shao, R.; Qu, Y.; He, Q.; Liu, L.; Yang, J. Spatial Full Degree-Of-Freedom Scattered Optical Field Modulation. *Laser Photonics Rev.* **2023**, *17* (9), No. 2300104.

https://doi.org/10.1021/acsphotonics.5c00816
ACS Photonics 2025, 12, 4423−4431